

## **FIELD VALIDATION OF BURNED AREA REFLECTANCE CLASSIFICATION (BARC) PRODUCTS FOR POST FIRE ASSESSMENT**

Andrew T. Hudak, Research Forester  
Peter R. Robichaud, Research Engineer  
Jeffrey S. Evans, Biologist/GIS Analyst  
USDA Forest Service, Rocky Mountain Research Station, Moscow, ID 83843  
[ahudak@fs.fed.us](mailto:ahudak@fs.fed.us), [jevans02@fs.fed.us](mailto:jevans02@fs.fed.us), [probichaud@fs.fed.us](mailto:probichaud@fs.fed.us)

Jess Clark, RS/GIS Analyst  
Keith Lannom, Operations Manager  
USDA Forest Service, Remote Sensing Applications Center, Salt Lake City, UT 84119  
[jtclark@fs.fed.us](mailto:jtclark@fs.fed.us), [klannom@fs.fed.us](mailto:klannom@fs.fed.us)

Penelope Morgan, Professor  
Carter Stone, GIS Analyst  
Department of Forest Resources, University of Idaho, Moscow, ID 83844-1133  
[pmorgan@uidaho.edu](mailto:pmorgan@uidaho.edu), [stonec@uidaho.edu](mailto:stonec@uidaho.edu)

**Abstract:** The USFS Remote Sensing Applications Center (RSAC) and the USGS EROS Data Center (EDC) produce Burned Area Reflectance Classification (BARC) maps for use by Burned Area Emergency Rehabilitation (BAER) teams in rapid response to wildfires. BAER teams desire maps indicative of soil burn severity, but photosynthetic and non-photosynthetic vegetation also influences the spectral properties of post-fire imagery. Our objective was to assess burn severity both remotely and on the ground at six 2003 wildfires. We analyzed fire-effects data from 34 field sites located across the full range of burn severities observed at the Black Mountain Two, Cooney Ridge, Robert, and Wedge Canyon wildfires in western Montana and the Old and Simi wildfires in southern California. We generated Normalized Burn Ratio (NBR), delta Normalized Burn Ratio (dNBR), and Normalized Difference Vegetation Index (NDVI) indices from Landsat 5, SPOT 4, ASTER, MASTER and MODIS imagery. Pearson correlations between the 44 image and 79 field variables having an absolute value greater than 0.5 were judged meaningful and tabulated in overstory, understory, surface cover, and soil infiltration categories. Vegetation variables produced a higher proportion of meaningful correlations than did surface cover variables, and soil infiltration variables the lowest proportion of meaningful correlations. Soil properties had little measurable influence on NBR, dNBR or NDVI, particularly in low and moderate severity burn areas where unconsumed vegetation occludes background reflectance. BAER teams should consider BARC products much more indicative of post-fire vegetation condition than soil condition. Image acquisition date, in relation to time of field data collection and time since fire, appears to be more important than type of imagery or index used. We recommend preserving the raw NBR or dNBR values in an archived map product to enable remote monitoring of post-fire vegetation recovery. We further recommend that BAER teams rely on the continuous BARC-Adjustable (BARC-A) product (and assign their own severity thresholds as needed) more than the classified BARC product, which oversimplifies highly heterogeneous burn severity characteristics on the ground.

### **INTRODUCTION**

The USDA Forest Service Remote Sensing Applications Center (RSAC) assists Burned Area Emergency Rehabilitation (BAER) teams responding to wildfires at a national scale by providing Burned Area Reflectance Classification (BARC) products derived from available satellite and airborne imagery. BARC products are derived from either the Normalized Burn Ratio (NBR) or delta NBR (dNBR) indices (Key and Benson, 2003b). Although dNBR is the default choice as a burn severity indicator, Bobbe et al. (2003), in a field validation of BARC products,

found dNBR to be no more accurate than NBR. Landsat imagery is the default choice for burn area mapping but SPOT, ASTER, MODIS and other imagery are important supplements.

There is a need to further assess the utility of the NBR and dNBR, and of the various image types, for burn severity mapping. We conducted an extensive field validation campaign at four wildfires in western Montana and two in southern California. Our objective was to assess how well NBR and dNBR, calculated from several image types, relate to a variety of field attributes with relevance to fire severity.

## METHODS

### Wildfires characterized

We characterized post-fire effects in the field, across the full range of fire severities, soon after six large wildfire events in 2003 (Fig. 1). The Black Mountain Two and Cooney Ridge wildfires, located west and east, respectively, of Missoula, Montana together burned over 10,000 ha through much of August and into September. Beginning in mid-July and for the next two months, the Robert and Wedge Canyon fires west of Glacier National Park burned nearly 45,000 ha combined. In less than two weeks from late October to early November, the Old and Simi wildfires north of San Bernadino and Simi Valley, respectively, collectively burned over 80,000 ha in southern California (Fig. 2).



Figure 1; Locations of six 2003 wildfires sampled in western Montana and southern California.

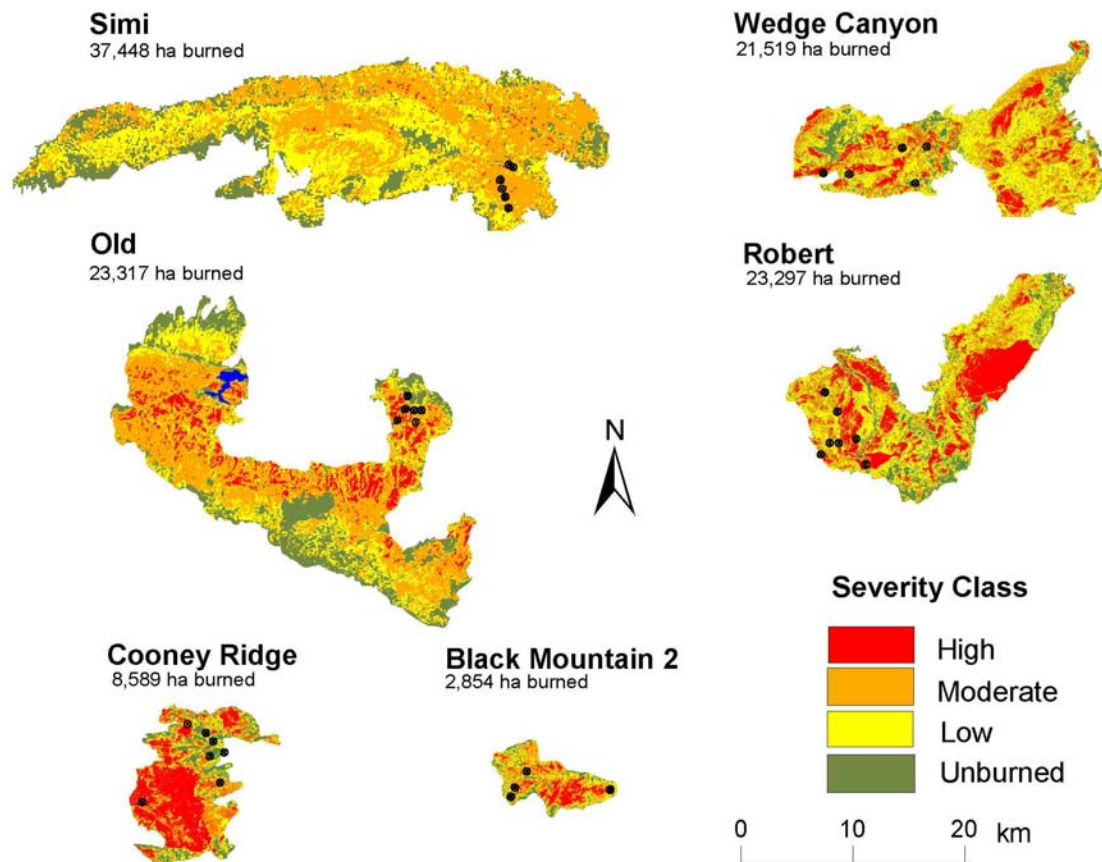


Figure 2; Burned Area Reflectance Classification (BARC) maps of the six 2003 wildfires sampled (Fig. 1), with 35 field sites plotted in black. At the Cooney Ridge fire, the easternmost site (on the fire perimeter) was excluded from the analysis because it burned after satellite image acquisition.

### Image Processing

The dNBR or, if pre-fire imagery is unavailable, the NBR, is used to produce the BARC product and the continuous, BARC-Adjustable (BARC-A) product from which the BARC map is derived. The BARC-A product is simply the continuous dNBR (or NBR) values stretched across the dynamic range of 8-bit data (0-255). Jenks Natural Breaks logic is used to assign breakpoints to the continuous BARC-A variable and produce the categorical BARC variable. Delivering the BARC-A product to BAER teams allows them to assign their own breakpoints based on ground observations. After classifying the BARC image, RSAC overlays the National Land Cover Database (NLCD) vegetation layer. Burned grasslands, for example, are often misclassified as “high” although grasslands rarely burn severely, and so cause little concern for BAER teams. RSAC thus uses the NLCD GIS overlay to catch any grassland areas classified as “high” during the NBR process and reclassifies them as “low.”

RSAC selects satellite images for mapping wildfires based on the availability of a cloud-free scene as soon as possible after the need for BARC products is identified. Landsat imagery is preferred for burn mapping due to its desirable temporal, spatial and spectral characteristics (Hudak et al. 2002). SPOT 4 has the advantage of being pointable, which enabled simultaneous acquisition of the Black Mountain and Cooney Ridge fires, and similarly the Robert and Wedge Canyon fires. However, SPOT imagery has the distinct disadvantage of being much more

expensive than Landsat (Clark et al. 2003). In addition, the substantial Landsat image archive greatly improves the possibility of obtaining a pre-fire image (acquired at approximately the same time of year) necessary for calculating dNBR, which is the currently preferred index for creating BARC products.

Landsat 5 or SPOT 4 images were available for the four Montana wildfires when needed. Timely SPOT 4 images were not available for the two southern California wildfires, and neither Landsat nor ASTER images were available when needed. RSAC thus turned to coarser spatial resolution MODIS imagery to initially map these fires and in the case of the Simi fire, to the airborne MASTER sensor based at the NASA Jet Propulsion Laboratory (Clark et al. 2003). Our six field sites at the Simi fire were situated just east of the Simi fire MODIS-derived BARC products, so we were unable to assess these, although we did calculate dNBR, NBR and NDVI indices from the MODIS image clipped to a larger extent. At the Old fire, our six field sites were located in the only cloud-free portion of a 3-Nov-03 Landsat 5 image, thus we calculated dNBR, NBR and NDVI indices even though no BARC-A product was made from this image. RSAC did produce BARC products from Landsat 5 and ASTER images when they later became available, in part to achieve a more complete assessment in this study (Table 1).

Table 1; Images used to generate dNBR, NBR and NDVI indices at the six wildfires sampled.

<b>Burn Area Imaged</b>	<b>Sensor Used</b>	<b>Pre-Fire Image Date</b>	<b>Post-Fire Image Date</b>	<b>Indices Calculated</b>	<b>BARC Products</b>
Black Mountain 2	Landsat-TM	10-Jul-02	25-Oct-03	dNBR, NBR, NDVI	dNBR
Black Mountain 2 / Cooney Ridge	SPOT-Xi		1-Sep-03	NBR, NDVI	NBR
Cooney Ridge	Landsat-TM	10-Jul-02	31-Aug-03	dNBR, NBR, NDVI	dNBR
Robert / Wedge Canyon	SPOT-Xi		10-Aug-03	NBR, NDVI	NBR
Robert / Wedge Canyon	Landsat-TM	21-Aug-00	25-Oct-03	dNBR, NBR, NDVI	dNBR
Old	Landsat-TM	7-Oct-02	3-Nov-03	dNBR, NBR, NDVI	
Old	ASTER	7-Oct-02 (TM)	18-Nov-03	dNBR, NBR, NDVI	dNBR
Old	Landsat-TM	7-Oct-02	19-Nov-03	dNBR, NBR, NDVI	dNBR
Old / Simi	MODIS	27-Sep-03	5-Nov-03	dNBR, NBR, NDVI	dNBR*
Simi	MODIS	27-Sep-03	28-Oct-03	dNBR, NBR, NDVI	
Simi	MASTER	12-Sep-02 (TM)	1-Nov-03	dNBR, NBR, NDVI	dNBR
Simi	Landsat-TM	12-Sep-02	10-Nov-03	dNBR, NBR, NDVI	dNBR

\*5-Nov-03 BARC products were only produced for the Old fire due to cloud cover over the Simi fire.

We assessed the NBR and dNBR indices, along with NDVI because of its immensely broad use in remote sensing of vegetation properties and potential applicability for burn severity mapping as well. The bands used to calculate these three indices depend on the type of sensor (Table 2) but follow the formulas,

$$\text{NBR} = (\text{NIR} - \text{SWIR}) / (\text{NIR} + \text{SWIR}) \quad (1)$$

$$\text{dNBR} = \text{NBR}_{\text{pre-fire}} - \text{NBR}_{\text{post-fire}} \quad (2)$$

$$\text{NDVI} = (\text{NIR} - \text{RED}) / (\text{NIR} + \text{RED}) \quad (3)$$

where RED denotes the red band, NIR denotes the near infrared band, and SWIR denotes the short wave infrared band. Input images received from RSAC were already georegistered and atmospherically corrected to at sensor reflectance. Output images of NBR, dNBR and NDVI were created in ERDAS Imagine, and pixel values at the field site locations were extracted in Arc/Info GRID.

Table 2; Characteristics of the spectral bands used to calculate dNBR, NBR and NDVI indices from the image types analyzed.

<b>Spectral Sensor</b>	<b>Spatial Resolution (m)</b>	<b>Red Band</b>	<b>Red Band Range (nm)</b>	<b>NIR Band</b>	<b>NIR Band Range (nm)</b>	<b>SWIR Band</b>	<b>SWIR Band Range (nm)</b>	<b>Fires Mapped</b>
ASTER	30	2	630-690	3	760-860	6	2185-2225	Old fire
Landsat-TM	30	3	630-690	4	760-900	7	2080-2350	All six fires
MASTER	31.5	5	630-690	9	845-885	21	2135-2185	Simi fire
MODIS	250	1	620-670	2	841-876	7	2105-2155	Two CA fires
SPOT-Xi	20	2	610-680	3	780-890	4	1580-1750	Four MT fires

### Field Data Collection

Field data were collected Sep-Oct (Montana) and Dec (California) of 2003 at 35 sites across 6 wildfires as follows: Black Mountain (4), Cooney Ridge (7), Robert (7), Wedge Canyon (5), Old (6) and Simi (6). One Cooney Ridge site was excluded because it burned only after the satellite images used in this analysis were acquired (Fig. 2). The 34 remaining sites spanned the full range of burn severities (low, moderate and high) at each wildfire. Burned sites were classified as low, moderate or high severity if tree crowns were predominantly green, brown or black, respectively. More low severity sites were sampled than moderate, and more moderate than high, because we noted while in the field that spatial heterogeneity in burn severity characteristics increased as burn severity decreased, confirming a finding of Turner et al. (1999).

Each site was centered 80-300 m from the nearest access road, in a random location within a broadly representative area of consistent stand and severity condition. At each site, nine 9 m x 9 m plots were situated along mutually bisecting transects in a 130 m x 130 m area. One transect was oriented along the prevailing slope with the other transect perpendicular to it, or across the slope. A plot was centered at the center and ends of each transect, 60 m from site center, with another plot centered in between 20, 30 or 40 m away. Each plot was comprised of fifteen 1 m x 1 m subplots arrayed in 3 rows with midlines spaced 4 m apart, while subplots in the same row were centered 2 m apart. Distances between plot centers were measured using a laser rangefinder, while subplot center points were measured using a cloth measuring tape and marked with reusable pin flags. Plot centers were geolocated with a Trimble GeoExplorer, logging a minimum of 150 positions, then subsequently differentially correcting and averaging them. Subplot positions were calculated based on their known, systematic distance and bearing from plot center.

At the subplot scale, fractional cover of green vegetation, rock, mineral soil, ash, litter (new and old) and any large organics was estimated ocularly, with the aid of a 1 m<sup>2</sup> square quadrat built from pvc pipe. Percent char of each cover component was also recorded. At the plot scale, a small ruler was used to measure depth of new litter (deposited post-fire), old litter and duff, and a convex spherical densiometer was used to measure canopy cover. Topographic features were also recorded. At every site, grass, forb, low shrub (greater than breast height) and seedling cover was estimated in a 1/750 ha circular plot, high shrubs (less than breast height) and saplings were tallied in a 1/100 ha plot, and trees and snags were inventoried in a 1/50 ha plot; these 3 vegetation plots were arranged concentrically at site center.

### Correlation Analysis

Measured and derived field variables were divided into overstory, understory, surface cover, and soil infiltration categories. Calculated spectral indices were divided into NBR, dNBR, NDVI, NBR-derived BARC-A and dNBR-derived BARC-A categories (Table 1). Correlation matrices between field and image variables were generated in R. Pearson correlation statistics were then compiled; correlations having absolute values greater than 0.5 were considered meaningful, and these were tallied within the field and image categories just named, as well as by sensor type and strength of correlation.

## RESULTS

Overstory and understory vegetation variables produced a higher proportion of meaningful correlations ( $r > 0.5$ ) with the spectral indices (Table 3,4), surface cover variables less (Table 5), and soil infiltration variables the lowest proportion (Table 6).

The ASTER sensor produced the highest proportion of meaningful correlations ( $r > 0.5$ ), followed by MASTER. Unfortunately, these images were only available for the Old and Simi fires, respectively, so it's difficult to separate the effect of sensor type from that of acquisition date. Not surprisingly, the coarser-resolution MODIS sensor produced the worst correlations among sensors (Fig. 3), while Landsat-TM and SPOT-Xi were intermediate.

NBR and dNBR burn severity indices produced a higher proportion of meaningful correlations ( $r > 0.5$ ) with the four field variable categories than did NDVI, except for the overstory category (Fig. 3). Comparing NBR and dNBR, dNBR did better than NBR in general, except for the overstory and surface cover categories. After comparing NBR and dNBR for several individual fires (e.g. Cooney Ridge, Fig. 5), NBR appeared to correlate better to field attributes when the post-fire image captured immediate post-fire effects. After several weeks have elapsed since burning, dNBR appeared to produce the better correlations.

When comparing burn areas imaged, Cooney Ridge produced the highest proportion of meaningful correlations ( $r > 0.5$ ), followed by the other Montana fires (Fig. 4). The California fires produced the worst relationships, but the lack of a tree overstory at many of the California field sites probably explains much of this difference.

Table 3; Overstory variables, ranked in descending order according to the number of meaningful correlations with image-derived spectral indices. Column tallies on the left are inclusive of column tallies on the right.

<b>Overstory Variables (N=21)</b>	<b>r &gt; 0.5</b>	<b>r &gt; 0.6</b>	<b>r &gt; 0.7</b>	<b>r &gt; 0.8</b>	<b>r &gt; 0.9</b>
Percent Crown Black	21	19	16	8	3
Plot Basal Area St. Dev.	14	12	12	11	6
Percent Overstory Cover Mean	14	12	10	9	6
Tree Height St. Dev.	14	9	7	6	2
Percent Crown Green	13	13	8	3	0
Crown Base Height Mean	12	9	6	2	1
Trees Per Hectare St. Dev.	12	8	5	5	2
Live Tree Count	9	8	5	3	0
Crown Base Height St. Dev.	9	8	5	1	0
Crown Base Height Minimum	9	8	5	1	0
Crown Base Height Maximum	9	7	7	7	2
Trees Per Hectare Sum	9	6	2	0	0
Tree Height Mean	9	4	2	0	0
Percent Crown Brown	8	7	5	2	1
Tree Height Minimum	8	6	4	0	0
Trees Per Hectare Mean	7	4	1	1	0
Plot Basal Area Mean	6	5	2	0	0
Tree Height Maximum	6	3	2	1	0
Plot Basal Area Sum	5	4	2	0	0
Percent Overstory Cover St. Dev.	4	1	0	0	0
Snag Count	3	3	3	2	2
<b>Total (924 possible)</b>	<b>201</b>	<b>156</b>	<b>109</b>	<b>62</b>	<b>25</b>
<b>Percentage</b>	<b>21.8</b>	<b>16.9</b>	<b>11.8</b>	<b>6.7</b>	<b>2.7</b>

Table 4; Understory variables, ranked in descending order according to the number of meaningful correlations with image-derived spectral indices. Column tallies on the left are inclusive of column tallies on the right.

<b>Understory Variables (N=22)</b>	<b>r &gt; 0.5</b>	<b>r &gt; 0.6</b>	<b>r &gt; 0.7</b>	<b>r &gt; 0.8</b>	<b>r &gt; 0.9</b>
Percent Grass Brown	27	18	7	3	2
Live High Shrub Count	24	17	9	1	0
Percent Grass Green	21	15	10	5	1
Live High Shrub Height Mean	20	11	5	0	0
Percent Low Shrub Brown	19	16	7	1	0
Dead High Shrub Count	19	12	7	5	1
Percent Saplings Dead	17	15	12	8	1
Dead Sapling Count	17	14	10	4	1
Percent Grass Black	16	12	7	6	1
Dead High Shrub Height Mean	12	6	3	3	2
Percent Low Shrub Black	11	10	7	2	2
Percent High Shrubs Dead	11	10	6	1	0
Dead Sapling Height Mean	10	5	3	2	0
Percent Forb Black	9	8	5	5	4
Percent Forb Green	9	5	2	2	1
Live Sapling Count	7	5	2	0	0
Live Sapling Height Mean	6	6	5	0	0
Percent Forb Brown	5	3	2	2	1
Percent Dead Seedling Cover	1	0	0	0	0
Percent Low Shrub Green	0	0	0	0	0
Percent Live Seedling Cover	0	0	0	0	0
Percent Seedlings Dead	0	0	0	0	0
<b>Total (968 possible)</b>	<b>261</b>	<b>188</b>	<b>109</b>	<b>50</b>	<b>17</b>
<b>Percentage</b>	<b>27.0</b>	<b>19.4</b>	<b>11.3</b>	<b>5.2</b>	<b>1.8</b>

Table 5; Surface cover variables, ranked in descending order according to the number of meaningful correlations with image-derived spectral indices. Column tallies on the left are inclusive of column tallies on the right.

<b>Surface Cover Variables (N=24)</b>	<b>r &gt; 0.5</b>	<b>r &gt; 0.6</b>	<b>r &gt; 0.7</b>	<b>r &gt; 0.8</b>	<b>r &gt; 0.9</b>
Depth Old Litter	14	11	4	3	0
New & Old Charred Cover	14	7	5	0	0
Depth Duff	13	7	4	1	0
New Litter Cover	12	6	0	0	0
Old Charred Cover	12	5	0	0	0
New & Old Uncharred Cover	11	6	0	0	0
Charred Inorganic Cover	11	1	0	0	0
Old Litter Cover	9	4	1	0	0
Uncharred Cover	9	1	0	0	0
Old Uncharred Cover	9	1	0	0	0
Uncharred Organic Cover	7	2	0	0	0
Depth New Litter	6	1	0	0	0
Charred Organic Cover	6	1	0	0	0
Mineral Soil Cover	4	0	0	0	0
Light Char Cover	4	0	0	0	0
Rock Cover	3	1	0	0	0
Moderate Char Cover	3	1	0	0	0

Uncharred Inorganic Cover	3	1	0	0	0
Old Green Cover	1	0	0	0	0
New Green Cover	0	0	0	0	0
Tree/Stump Cover	0	0	0	0	0
Ash Cover	0	0	0	0	0
Deep Char Cover	0	0	0	0	0
New & Old Green Cover	0	0	0	0	0
<b>Total (1056 possible)</b>	<b>151</b>	<b>56</b>	<b>14</b>	<b>4</b>	<b>0</b>
<b>Percentage</b>	<b>14.3</b>	<b>5.3</b>	<b>1.3</b>	<b>0.4</b>	<b>0.0</b>

Table 6; Soil infiltration variables, ranked in descending order according to the number of meaningful correlations with image-derived spectral indices. Column tallies on the left are inclusive of column tallies on the right.

<b>Soil Infiltration Variables (N=12)</b>	<b>r &gt; 0.5</b>	<b>r &gt; 0.6</b>	<b>r &gt; 0.7</b>	<b>r &gt; 0.8</b>	<b>r &gt; 0.9</b>
Infiltration start time - deep char	14	6	3	0	0
Infiltration rate - deep char	11	8	5	3	0
Infiltration rate - uncharred	8	6	3	0	0
Water Drop Point Test - deep char	8	5	1	1	0
Water Drop Point Test - uncharred	7	4	0	0	0
Infiltration start time - uncharred	1	0	0	0	0
Infiltration start time - moderate char	0	0	0	0	0
Infiltration rate - moderate char	0	0	0	0	0
Water Drop Point Test - moderate char	0	0	0	0	0
Infiltration start time - light char	0	0	0	0	0
Infiltration rate - light char	0	0	0	0	0
Water Drop Point Test - light char	0	0	0	0	0
<b>Total (528 possible)</b>	<b>49</b>	<b>29</b>	<b>12</b>	<b>4</b>	<b>0</b>
<b>Percentage</b>	<b>9.3</b>	<b>5.5</b>	<b>2.3</b>	<b>0.8</b>	<b>0.0</b>

## DISCUSSION

These results strongly suggest that BARC maps should be considered more indicative of vegetation severity than soil severity, as they often have been (Parsons and Orlemann 2002). It is not surprising that the spectral indices derived from overhead imagery should correlate better to vegetation than soil variables because the vegetation occludes the ground. Similarly, a higher proportion of surface cover variables should correlate meaningfully than soil infiltration variables, because the reflectance signal is more influenced by areal cover fractions than by an essentially point measure of a soil process such as water penetrability.

Spectral mixture analysis is therefore a sensible image processing strategy to estimate green and nonphotosynthetic vegetation, litter and soil fractions directly from the imagery, and we will pursue this with post-fire hyperspectral imagery acquired over all 35 field sites. The broad array of field variables will thus serve as valuable ground truth data for validating fractional cover estimates and to quantify to what degree vegetation variables have more influence on moderate, or especially, low burn severities compared to high burn severity.

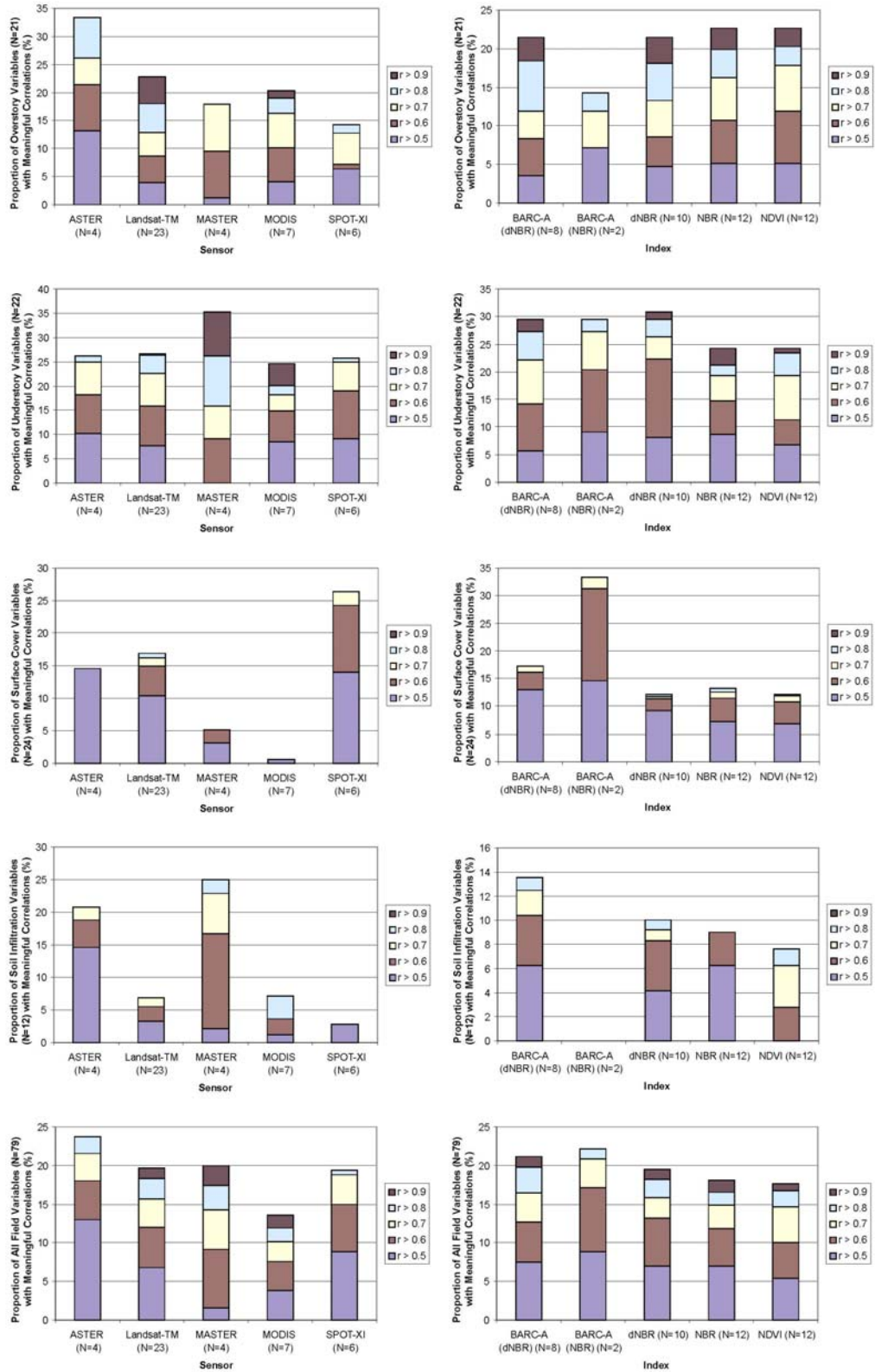


Figure 3; Field variables, categorized as in Tables 3-6, with meaningful correlations to spectral indices, categorized by sensor type (left) and index type (right) (Table 1). Column height represents the cumulative sum of meaningful correlations ( $r > 0.5$ ).

Some field variables of post-fire effects are much more temporally dynamic than others. Ash cover proved a poor correlate probably because it is redistributed by wind and water quickly following fire. Green vegetation regrowth is another dynamic phenomenon, as is needlecast (new litter) on moderate severity burns. At Black Mountain Two and Cooney Ridge, bear grass and other green vegetation had not yet resprouted, nor had most of the scorched needles fallen, at the time of satellite image acquisition. Moreover, most field sites were placed soon after the fire, which very likely explains the stronger correlations at these wildfires (Figs. 3,4). In future analyses, dates will be extracted from fire progression data to measure time elapsed from burning until the data were acquired by the remote sensor or collected in the field, to better evaluate the importance of the timeliness of image and field data acquisition.

Cooney Ridge was also advantageous for comparing indices derived from Landsat-TM and SPOT-Xi, because the respective scenes were acquired only a day apart (Table 2, Fig. 5). The NBR appears to produce better correlations if the image is acquired soon after burning, before conditions change. As time since fire increases, the dNBR appears to become more useful. In a prior study mapping burn areas in rangelands, Hudak et al. (2002) found that after a growing season, some burn areas could not be reliably delineated without the addition of a pre-fire image.

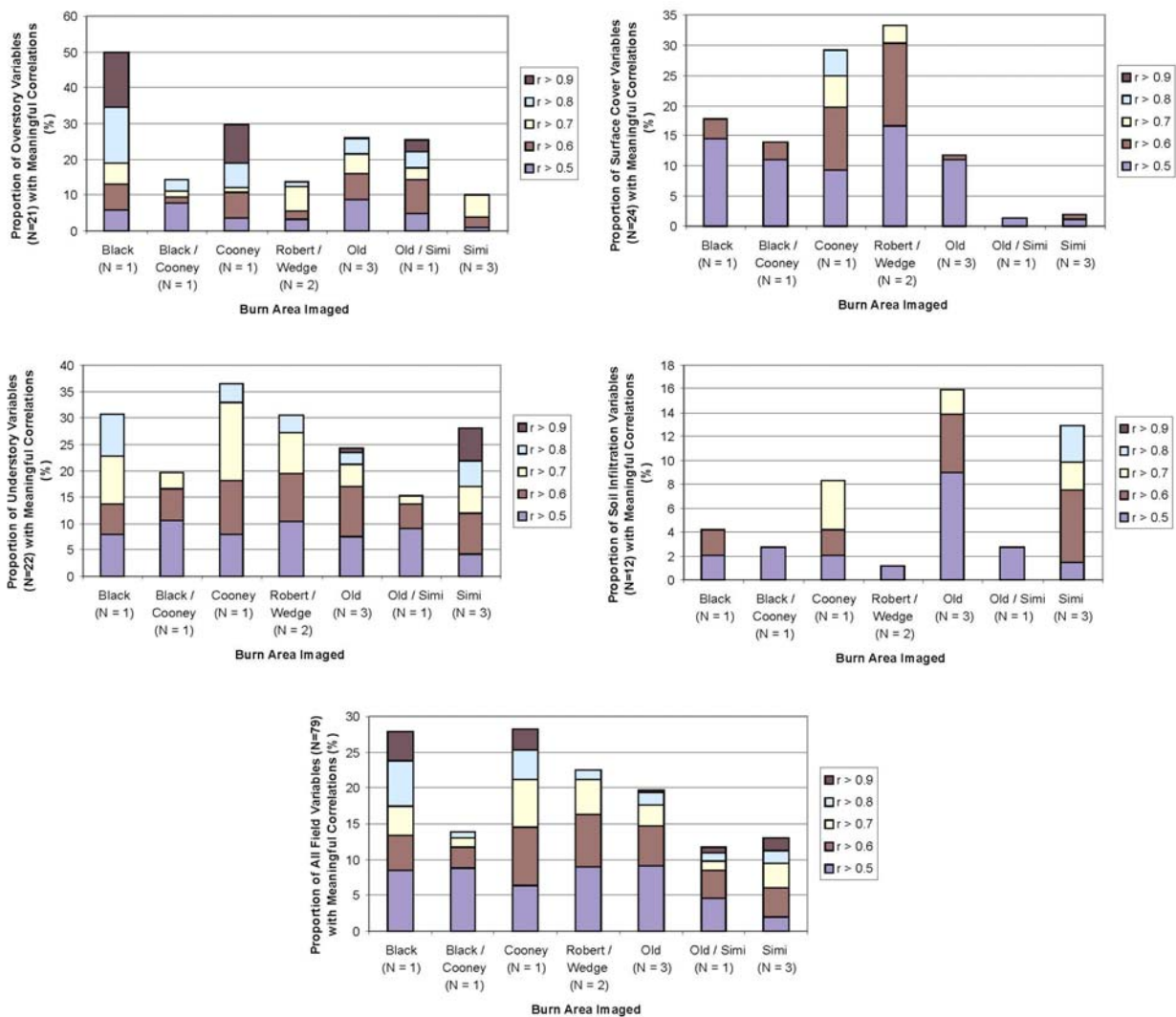


Figure 4; Field variables, categorized as in Tables 3-6, with meaningful correlations to spectral indices, categorized by burn area imaged in a single acquisition (Table 1). Column height represents the cumulative sum of meaningful correlations ( $r > 0.5$ ).

Rescaling the raw indices to produce the 0-255 BARC-A values changed the correlations but not to an important degree. The higher proportion of meaningful BARC-A correlations (Fig. 3) is a consequence of a higher number of raw indices being generated from images judged suboptimal, or otherwise not used for BARC products. There is no reason to expect the rescaling to consistently improve correlations to field attributes. A great disadvantage of the rescaling is that it subtracts value from the BARC products, making BARC-A values incomparable between fire events. We recommend that RSAC archive NBR and dNBR (if available) products, for the added value of monitoring post-fire recovery.

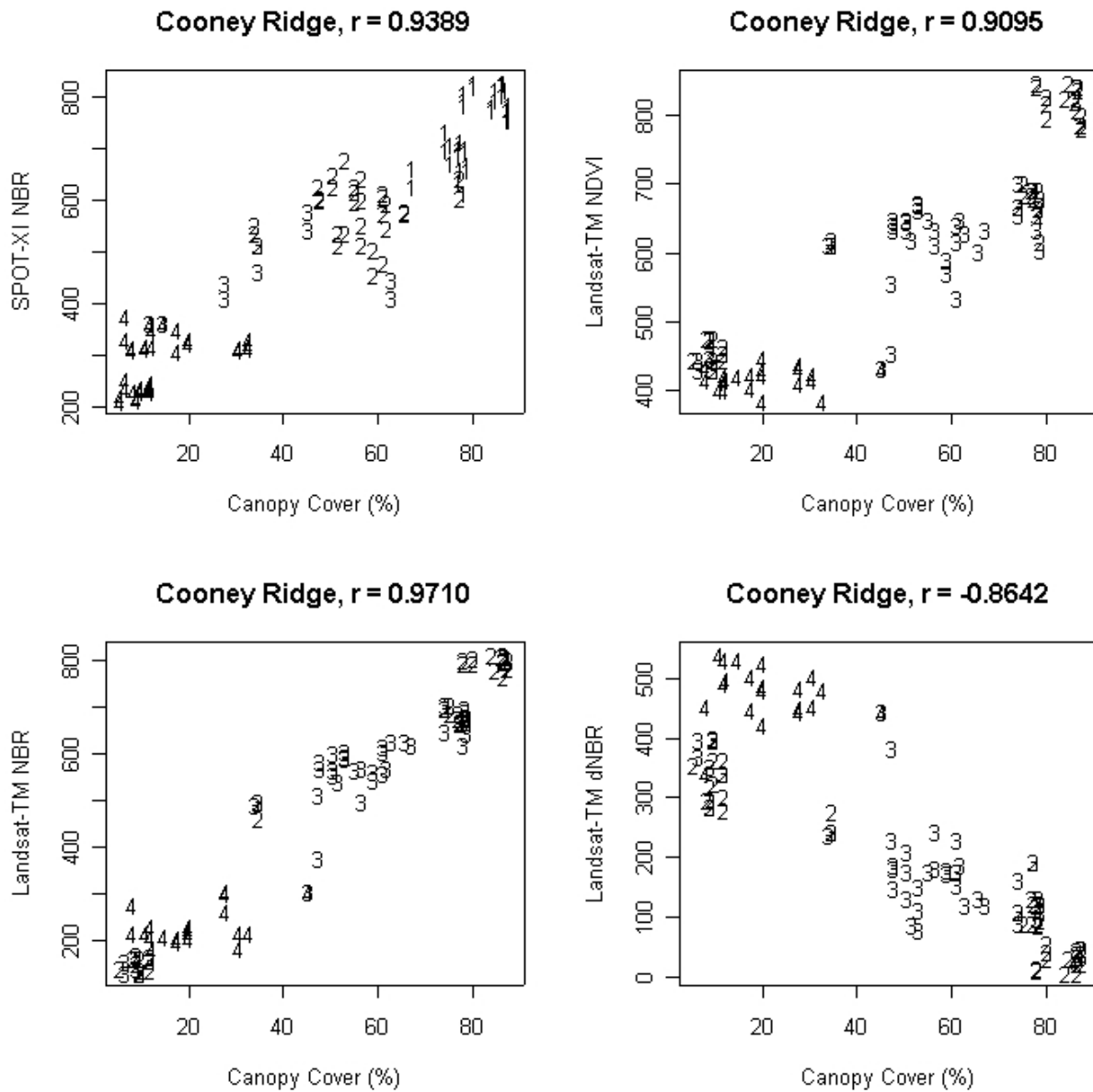


Figure 5; Scatterplots and Pearson correlations of canopy cover vs. SPOT-XI NBR, Landsat-TM NDVI, Landsat-TM NBR and Landsat-TM dNBR, based on six Cooney Ridge sites. Numbers in scatterplots denote BARC classes (4 = high, 3 = moderate, 2 = low, 1 = unburned).

## CONCLUSION

Burn severity characteristics in the field are extremely heterogeneous, and all vary continuously across scales. During the 2003 fire season, RSAC analysts produced a preliminary color classification of the BARC-A product using Jenks Natural Breaks logic. This was not meant to represent accurate breakpoints between severity classes, but to provide field users with an easier starting point for classification than a grayscale image. However, these breakpoints often bared little resemblance to burn severity characteristics on the ground. Therefore, to produce the preliminary BARC-A color classification during the 2004 fire season, RSAC instead will apply breakpoints according to Key and Benson (2003a), which better relates NBR or dNBR to burn severity characteristics on the ground. We encourage BAER teams to rely more on the continuous BARC-A product than the classified BARC product, because it is the users on the ground who are best suited to assign appropriate breakpoints to the BARC-A product as they consider useful.

## REFERENCES

- Bobbe, T., M. V. Finco, B. Quayle, K. Lannom, R. Sohlberg and A. Parsons (2003). Field measurements for the training and validation of burn severity maps from spaceborne, remotely sensed imagery. Final Project Report, Joint Fire Science Program-2001-2, 15 p.
- Clark, J., A. Parsons, T. Zajkowski and K. Lannom (2003). Remote sensing imagery support for Burned Area Emergency Response teams on 2003 southern California wildfires. USFS Remote Sensing Applications Center BAER Support Summary, 25 p.
- Hudak, A., P. Morgan, C. Stone, P. Robichaud, T. Jain and J. Clark (2004). The relationship of field burn severity measures to satellite-derived Burned Area Reflectance Classification (BARC) maps. *International Archives of Photogrammetry and Remote Sensing*, submitted.
- Hudak, A. T. and B. H. Brockett (2002). Rangeland fire scar mapping using Landsat imagery. *Proceedings of the Ninth Biennial Forest Service Remote Sensing Applications Conference*, CD-ROM.
- Key C. H. and N. C. Benson (2003a). The Composite Burn Index (CBI): field rating of burn severity. <http://nrm-sc.usgs.gov/research/cbi.htm>
- Key, C. H. and N. C. Benson (2003b). The Normalized Burn Ratio, a Landsat TM radiometric index of burn severity. <http://nrm-sc.usgs.gov/research/ndbr.htm>
- Parsons, A. and A. Orlemann (2002). Burned Area Emergency Rehabilitation (BAER)/Emergency Stabilization and Rehabilitation (ESR). Burn Severity Definitions/Guidelines Draft Version 1.5, 27 p.
- Roberts, D. A., M. O. Smith and J. B. Adams (1993). Green vegetation, non-photosynthetic vegetation and soils in AVIRIS data. *Remote Sensing of Environment* 44: 255-269.
- Turner, M. G., W. H. Romme and R. H. Gardner (1999). Prefire heterogeneity, fire severity, and early postfire plant reestablishment in subalpine forests of Yellowstone National Park, Wyoming. *International Journal of Wildland Fire* 9: 21-36.